ADVANCES IN EXPERIMENTAL VERIFICATION OF REMOTE SPACECRAFT ATTITUDE CONTROL BY COULOMB CHARGING

Daan Stevenson and Hanspeter Schaub

GNC 2014: 9th International ESA Conference on Guidance, Navigation & Control Systems
Porto, Portugal | 2 - 6 June 2014
European Space Agency

GNC 2014: 9th International ESA Conference on Guidance, Navigation & Control Systems
Porto, Portugal | 2 - 6 June 2014
European Space Agency

ADVANCES IN EXPERIMENTAL VERIFICATION OF REMOTE SPACECRAFT ATTITUDE CONTROL BY COULOMB CHARGING

D. Stevenson[1] and H. Schaub[2]
[1,2]University of Colorado Boulder, USA

ABSTRACT

In order to ameliorate the ever increasing space situational awareness risks at Geosynchronous (GEO) orbits, spacecraft rendezvous is desirable for servicing or repositioning operations. When large GEO spacecraft loose station keeping control, they can acquire sizable rotational momenta that imperil proximity operations and docking. Remote electrostatic charge control has been identified as a technology that may be used to safely despin non-spherical objects over a period of time. The Coulomb torques that are produced can be modeled by the recently developed Multi-Sphere Method or approximated analytically. Nonlinear stability arguments are made for control algorithms that achieve a desired rotation rate or specific attitude control in one dimension. An enhanced experimental testbed has been constructed to support this technology development. High voltage power supplies control the electrostatic potential on a conducting cylinder that rotates freely about its minor axis and on a stationary control sphere located in close proximity. Using only the Coulomb interaction, the system is able to swiftly bring the cylinder to rest from a large rotation rate, and position it in a desired angular orientation.

1. INTRODUCTION

The use of electrostatic actuation for spacecraft relative motion control has received extensive attention in the literature over the past decades [1, 2, 3]. In the Geosynchronous Orbit (GEO) environment, the favorable space plasma conditions allow for relatively low current emission to maintain non-equilibrium potentials on space objects, yielding power requirements on the order of Watts [4]. Due to the minimal mass emission of charge control devices, Coulomb actuation is essentially propellant-less and plume impingement issues associated with the use of conventional thrusters in close proximity spacecraft formations are avoided. If a spacecraft can impart relative potentials on itself and an inactive craft using a focused charged beam, touchless electrostatic maneuvers may be achieved within non-cooperative formations [5, 6]. This technology is applicable to various mission scenarios intended to ameliorate the expanding orbital debris situation at GEO [7, 8, 9, 10]. For example, an attractive electrostatic force can act as a virtual tether between the two craft, while a low thrust maneuver is used to tow the non-cooperative object into a new orbit [11, 12].

While this approach can be used to increase the semi-major axis of a GEO debris object by 300 km in two months, a docked Hohmann transfer would accomplish this in just over 12 hours. Rendezvous with debris objects is complicated by the fact that uncontrolled GEO satellites may exhibit rotation rates up to 10 deg/s [13]. Meanwhile, pose algorithms and attitude matching maneuvers for rendezvous are generally restricted to rotation rates below 1 deg/s [14, 15], thus limiting the viable targets for a physical docking strategy. Because non-cooperative spacecraft at GEO often exhibit large moments of inertia and angular momenta, a touchless method for reducing the rotation rate prior to rendezvous is desired. Investigation of the charged Coulomb interaction between non-spherical bodies suggests that prolate bodies can experience torques and off-axis forces [16]. If these torques can be harnessed to remotely decrease the rotation

of the target as depicted in Fig. 1, the trade space of candidate spacecraft for rendezvous and docking operations is greatly increased. An alternative to repositioning derelict satellites into a graveyard orbit is to service them by replenishing fuel reserves or repairing failed components. Such missions, as investigated by NASA's Satellite Servicing Capability Office and DARPA's Phoenix program, preclude the unnecessary insertion of replacement satellites.

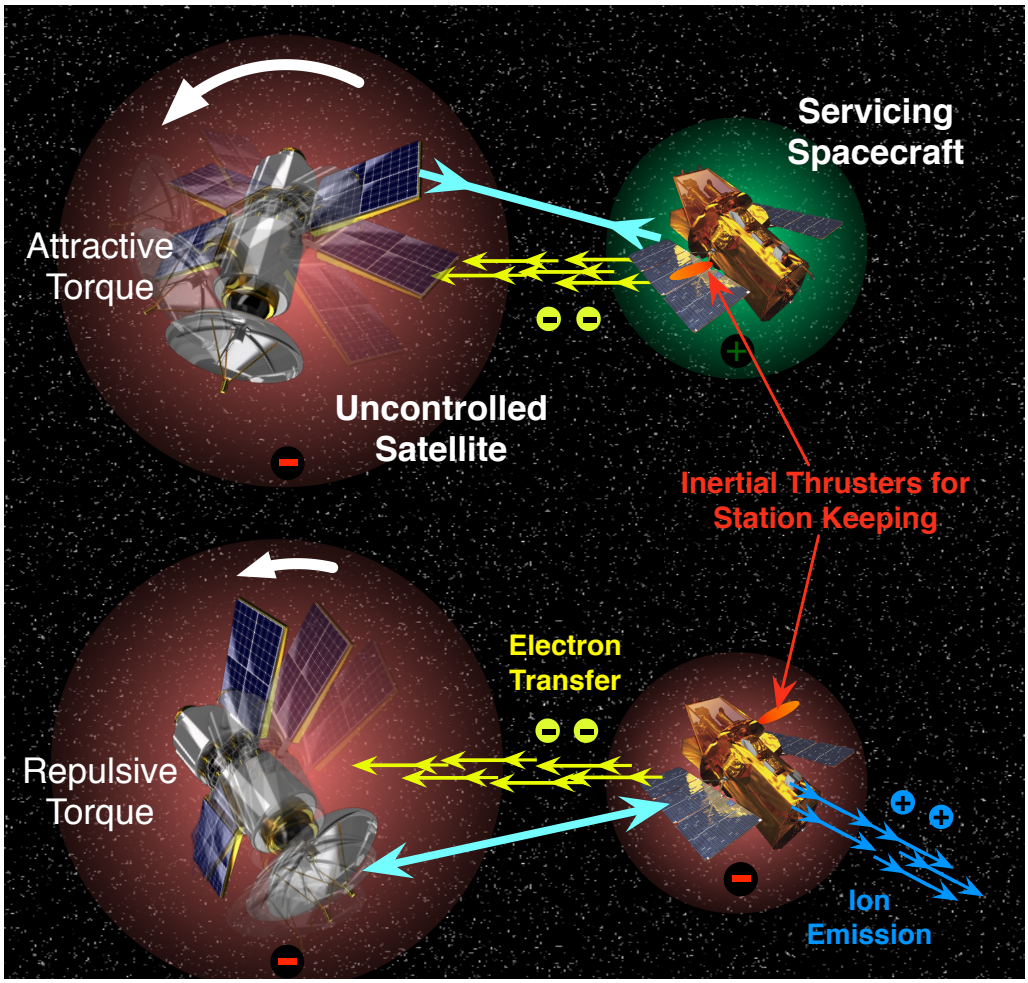

Fig. 1: *Electrostatic actuation technology enabling diverse service mission profiles*

The touchless electrostatic despin concept requires the servicing craft to actively control its own electrostatic potential through the use of an electron and/or ion gun. If the charged emission is aimed at the target object, the potentials of both craft can be controlled [17]. The goal is to attract the tumbling target's closest receding feature and repel its closest approaching feature, thereby despinning the spacecraft over time. While aspects of the 3D control problem are being investigated [18], the scope of this work considers one-dimensional rotational motion. This is a good assumption for many GEO debris objects, which rotate in a minimum energy state flat spin due to decades of internal energy dissipation. The non-spherical, tumbling space body is assumed to be cylindrical, which is representative of many upper stage rocket bodies such as the Centaur. Meanwhile, the non-tumbling control vehicle is chosen to be spherical in shape. Previous studies identify the system's equilibrium orientations and focus on Lyapunov stable nonlinear control strategies to arrest the rotation of the uncontrolled body [19]. These strategies have been verified with numerical simulations, while simple rate control algorithms have been tested on a rotational Coulomb charge control testbed [20]. This paper extends these efforts to develop control algorithms that prescribe a specific non-equilibrium attitude

on the uncontrolled body, and validate these algorithms on the improved experimental testbed. Executing absolute attitude control prior to precise docking maneuvers greatly reduces collision risks and guidance and control challenges during rendezvous.

2. EXPERIMENTAL SETUP

A. Testbed Description

A prototype testbed allowing rotational Coulomb charge control experiments was first introduced in [20]. While this testbed demonstrated that touchless spin control experiments are feasible in a 1-G atmospheric environment, several hardware limitations were identified in this setup that restricted the performance to rotation rate control only. First, knowledge of the rotating object's angular positions was collected using a range-finding laser, which yielded noisy attitude data with insufficient accuracy. Second, active charge control was not implemented on the rotating cylinder. Rather, an initial voltage was applied to the cylinder whose gradual charge drain was characterized and modeled in the simulations. This resulted in a lack of repeatability and an inability to modulate the voltage on the cylinder during the experiment for precise control of the Coulomb torques. Lastly, the high voltage power supplies exhibited a time delay of up to one second when switching voltage polarity, thus considerably reducing the control authority in the case of large rotation rates.

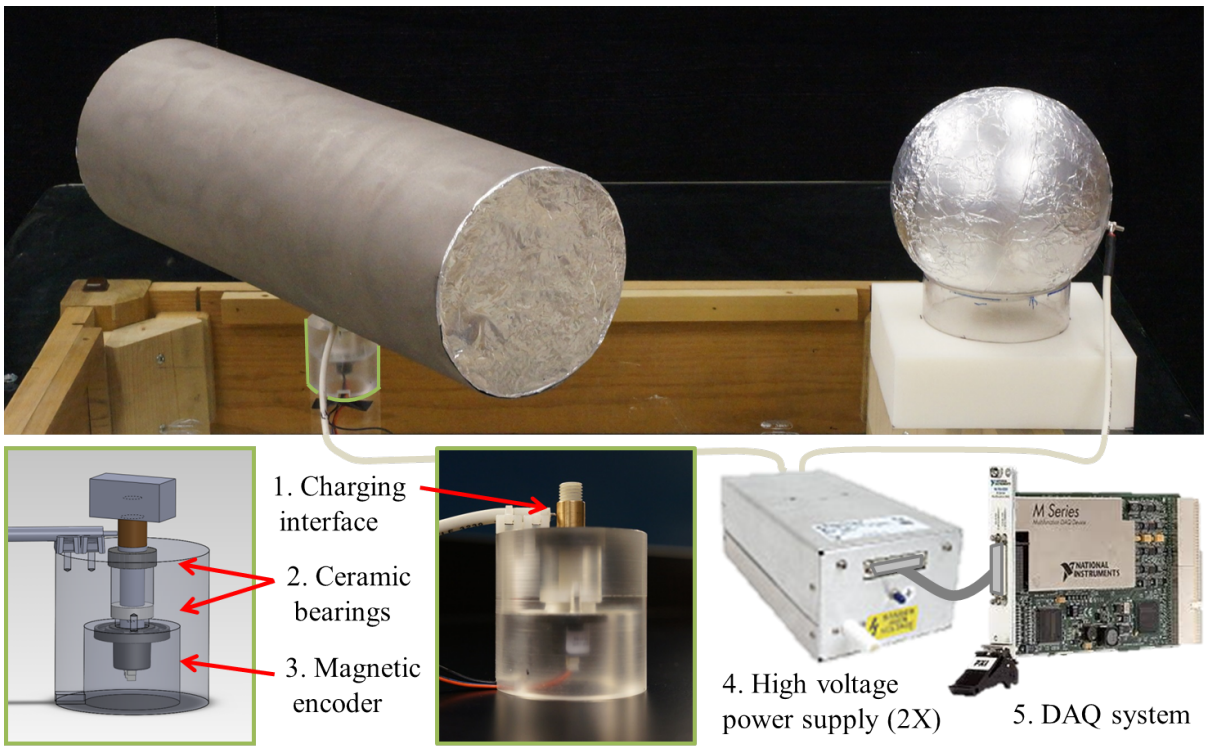

Fig. 2: *Depiction of the experimental setup for charged attitude control*

Fig. 2 depicts the improved rotational testbed for Coulomb attitude control experiments, wherein all the above limitations are addressed. The conducting cylinder is attached with a threaded interface to a rotating shaft, which is secured by the two low friction ceramic bearings. A magnetic hub is mounted to the bottom of the shaft, whose orientation is measured to within 0.35° accuracy by the absolute 10-bit analog encoder. Analysis and testing suggests that the magnetic fields produced by the charged rotating cylinder are sufficiently small and do not interfere with the operation of the encoder. Charge is transfered to the rotating cylinder from a Spellman CZE

2000 high voltage power supply (HVPS) via a < 1 mm gap between the charging cable and a copper bushing situated on the rotating shaft. This results in ionization of the surrounding air, effectively reducing its dielectric breakdown voltage. To prevent electrical damage to the magnetic encoder in the case of an electrostatic discharge, a grounding cable is mounted underneath the encoder. The stationary sphere, which experiences frequent polarity changes when using the charge control algorithms developed below, is charged using the Masusada CZ9-30R power supply, which exhibits an order of magnitude quicker polarity switching, with verified delays lower than 0.1 seconds. Both power supplies are capable of supplying ± 30 kV at up to 300 μA, which results in power levels well within typical safety limits when proper precaution measures are practiced.

Input and output control for the power supplies and angular encoder is achieved by a PCI express based 16-Bit multi-channel NI DAQ card. National Instruments LabVIEW software is utilized to monitor and interact with the hardware. Data sampling at 66.66 Hz is achieved, which far exceeds the time constants evident in the dynamics of the system. Differentiation of the cylinder's angular position is performed within LabVIEW using a discrete derivative with switching logic to handle the multiple revolution discontinuity, which is passed through a third order lowpass Chebyshev filter. The custom graphical user interface shown in Fig. 3 allows for various operation modes, including manual voltage control, angular position control, and rotation rate control.

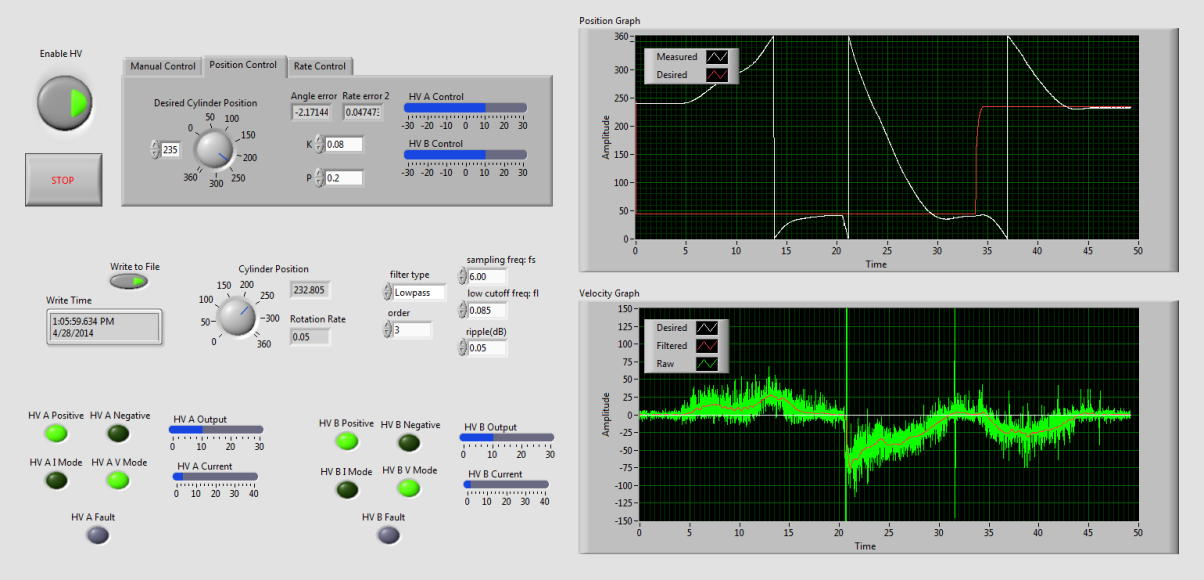

Fig. 3: *Screenshot of the LabVIEW graphical user interface*

B. DISTURBANCE CHARACTERIZATION

As with the previous experimental setup, the two disturbance torques that act on the rotating cylinder are a constant friction torque from the ceramic bearings M_b and a rotation rate dependent atmospheric drag torque M_d. As derived in [20], these torques are given by the following expressions, where F_a is the axial force acting on the bearings from the weight of the cylinder, $\rho = 1.194$ kg/m^3 is a typical atmospheric air density, D and L are the diameter and length of the cylinder, and $\dot{\theta}$ is its rotation rate in rad/s. The remaining parameters, the bearing friction

coefficient C_b and the cylinder drag coefficient C_d are to be determined empirically.

$$M_b = C_b F_a \tag{1}$$

$$M_d = \frac{\rho \dot{\theta}^2 C_d D L^4}{64} \tag{2}$$

Five sets of data are collected by giving the cylinder an initial rotation and allowing it to de-spin naturally while the electric potential on both the cylinder and the adjacent sphere are held at zero. Fig. 4(a) shows the angular rates of the cylinder for each experimental run and a simulated de-spin using the modeled disturbance torques from Eq. (1) and (2). The corresponding coefficients were tuned until the resultant angular velocity curve optimally fit the experimental data, resulting in $C_b = 0.000024$ and $C_d = 0.92$. Fig. 4(b) shows the resulting disturbance torques in the simulation, suggesting that the drag force is dominant at angular rates higher than 33 deg/s.

(a) Angular velocity, simulated and experimental

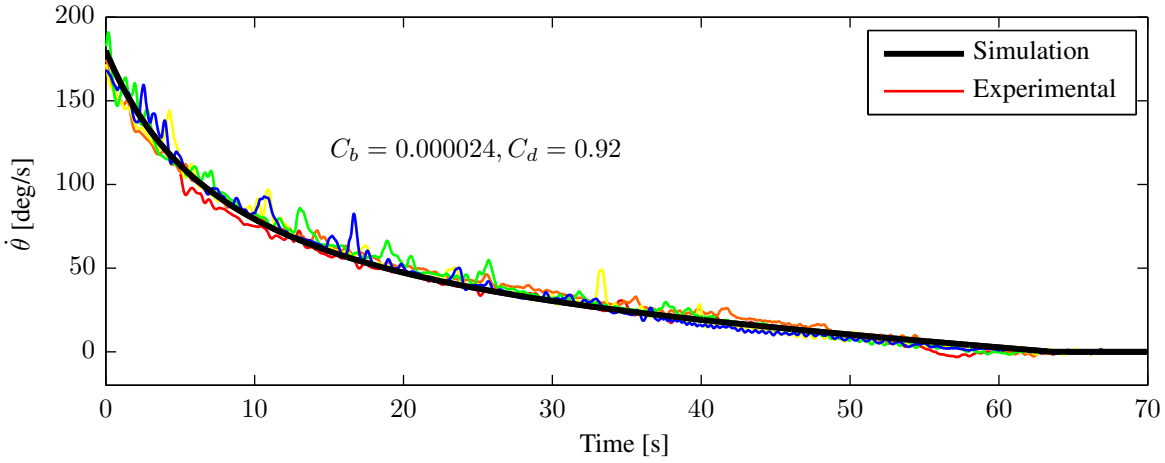

(b) Disturbance torques, simulated

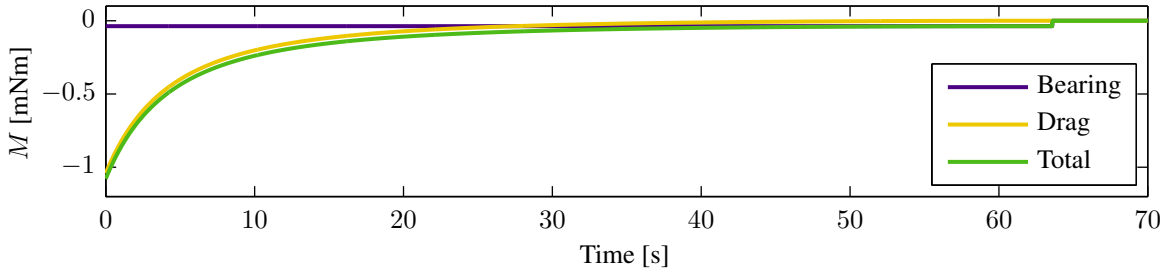

Fig. 4: *Characterization of disturbance torques*

3. MULTI-SPHERE METHOD

To predict first order electrostatic interaction, charged spacecraft can be modeled by point charges [21] or by conducting spheres [22]. Since these methods lack the ability to resolve the charge distribution on non-symmetric bodies, they are incapable of predicting electrostatic torques and off-axis forces. Meanwhile, highly accurate numerical solutions are possible by Finite Element Analysis (FEA), but this approach lacks the computational speed necessary for faster-than-realtime 6 Degree of Freedom (6DOF) charged relative motion simulations. The

recently developed Multi-Sphere Method (MSM) uses a set of conductive spheres throughout the geometry of a spacecraft to capture the 3D electrostatic effects, thus achieving the desired balance between computational efficiency and accuracy [23]. The framework is presented here as applied to the cylinder-sphere system shown in Fig. 5. While it is possible to capture the induced charge effects that occur at very close separation distances with a larger set of spheres distributed on the surface of the objects [24], three spheres are sufficient to capture the torques exerted on the cylinder in the experimental configuration.

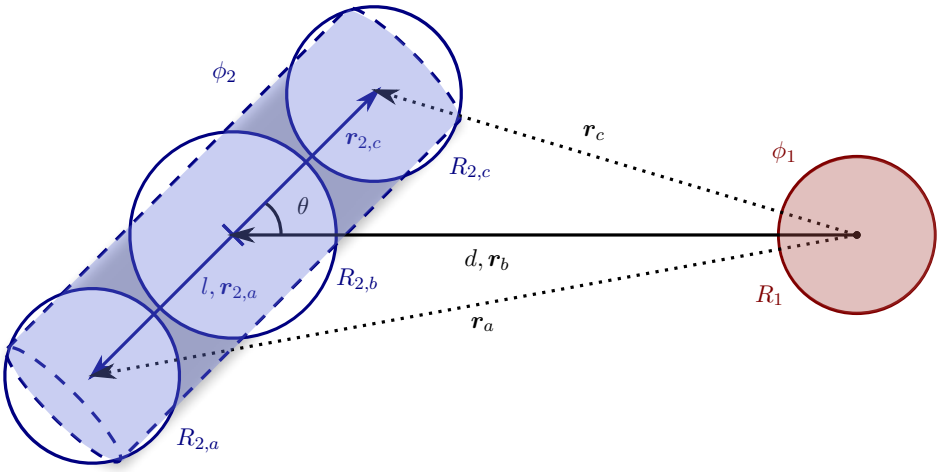

Fig. 5: *3-sphere MSM for cylinder-sphere configuration*

The defining system parameters are the separation distance d, the cylinder orientation angle θ, and the control voltages ϕ_1 and ϕ_2. In the experimental testbed, the cylinder has a 15 cm diameter and a 45 cm length. The mass of the rotating components is 156.8 g, with a transverse moment of inertia of 2.867 g·m^2. The 15 cm diameter stationary sphere has a 15 cm surface to surface separation from the cylinder at a parallel orientation with $\theta = 0°$. Table 1 gives the dimensions as outlined in Figure 5, where the MSM parameters are scaled down from the optimized set found in Ref. [23].

Table 1: *Parameters for cylinder attitude control system*

Parameter	Value	Units	Description
m_{cyl}	156.8	g	Cylinder mass
I_{cyl}	2.867	g·m^2	Cylinder transverse moment of inertia
d	45	cm	Object center-to-center separation
l	17.353	cm	MSM Parameters
R_a, R_c	8.8634	cm	MSM Parameters
R_b	9.7664	cm	MSM Parameters

The electrostatic forces are determined by the charges residing on each sphere. These result from the prescribed electric potentials, according to the self and mutual capacitance relationship in Eq. (3), where $k_c = 8.99 \times 10^9$ Nm^2/C^2 is Coulomb's constant: [25, 26, 22]

$$\phi_i = k_c \frac{q_i}{R_i} + \sum_{j=1, j\neq i}^{m} k_c \frac{q_j}{r_{i,j}} \tag{3}$$

These relations can be combined for each sphere to obtain the matrix equation

$$\begin{bmatrix} \phi_1 \\ \phi_2 \\ \phi_2 \\ \phi_2 \end{bmatrix} = k_c \underbrace{\begin{bmatrix} 1/R_1 & 1/r_a & 1/r_b & 1/r_c \\ 1/r_a & 1/R_{2,a} & 1/l & 1/2l \\ 1/r_b & 1/l & 1/R_{2,b} & 1/l \\ 1/r_c & 1/2l & 1/l & 1/R_{2,c} \end{bmatrix}}_{[C_M]^{-1}} \begin{bmatrix} q_1 \\ q_a \\ q_b \\ q_c \end{bmatrix} \tag{4}$$

By inverting $[C_M]^{-1}$, the charge on each sphere is determined at any instance of time. The total electrostatic force and torque about the center of the cylinder are then given by the summations

$$\boldsymbol{F}_2 = k_c q_1 \sum_{i=a}^{c} \frac{q_i}{{r_i}^3} \boldsymbol{r}_i \tag{5}$$

$$\boldsymbol{M}_2 = k_c q_1 \sum_{i=a}^{c} \frac{q_i}{{r_i}^3} \boldsymbol{r}_{2,i} \times \boldsymbol{r}_i \tag{6}$$

Meanwhile, there is a net attractive or repulsive force acting between the two objects in the system. In space, the control craft (the sphere) must create a thrusting force to oppose this Coulomb interaction, thus providing the external influence needed to remove the cylinder's angular momentum from the system. In the terrestrial experiment, the sphere mount and cylinder bearings provide the constraints necessary to oppose these Coulomb forces.

4. SYSTEM DYNAMICS

While the Multi-Sphere Method is proficient for predicting cylinder torques given the necessary orientation and voltage parameters, the nonlinear algorithms involved are not readily invertible. For control purposes, it is advantageous to determine what voltage is required to provide a desired torque at a specific cylinder orientation. Without loss of generality, it is assumed that the voltage applied to the control sphere is $\phi_1 = \phi$ and the voltage applied to the cylinder is $\phi_2 = |\phi_1|$. As a result, negative ϕ implies opposite polarity, attractive control while positive ϕ implies equal polarity, repulsive control. Fig. 6 shows the Coulomb torque M_C exerted on the cylinder for various cylinder orientations and applied potentials. This data could be used as a lookup table to determine the necessary potentials for a desired torque, but for nonlinear stability analysis, a more analytic formulation is desired.

In [19], it is assumed that the separation distance is sufficiently large for the induced charging effects to be negligible. The Coulomb torque on the cylinder is then modeled using the analytic expression

$$M_C = \gamma f(\phi) g(\theta) \tag{7}$$

where

$$f(\phi) = \phi|\phi| \tag{8}$$

and

$$g(\theta) = \sin 2\theta \tag{9}$$

From the asymmetry in Fig. 6, it is clear that the formulation above does not hold for the configuration in the experimental testbed. Due to the proximity of the shapes and the resulting induced charging effect, the torques produced by the attractive configuration are considerably

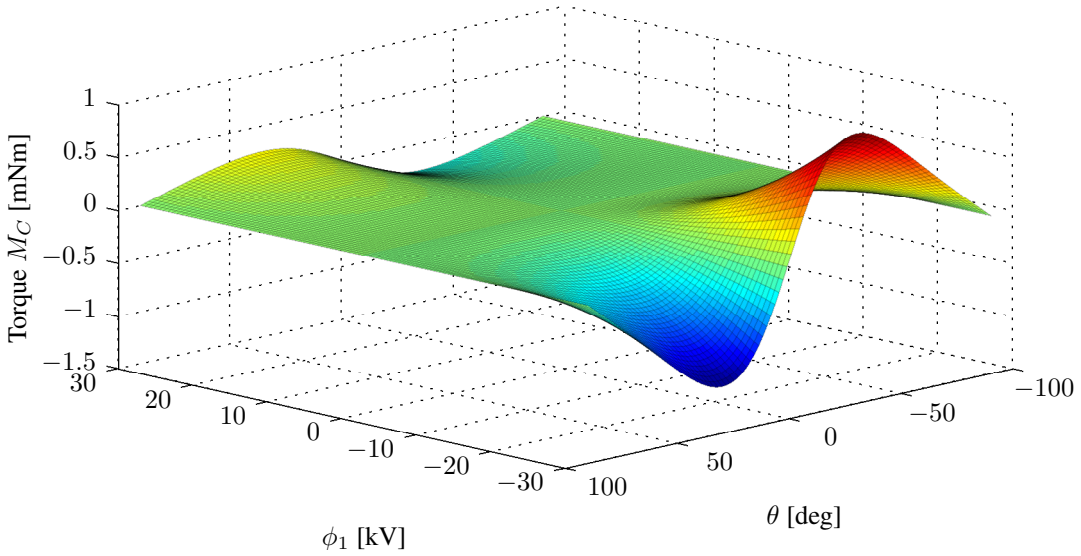

Fig. 6: *Coulomb torques for various orientations and potentials of the charged rotational testbed*

larger than those imparted by electrostatic repulsion. To capture this asymmetry, a polarity dependent coefficient $\gamma(\text{sign}(\phi))$ is proposed, where γ remains always positive:

$$\gamma(\text{sign}(\phi)) = \begin{cases} \gamma_a & \text{for } \phi < 0 \\ \gamma_r & \text{for } \phi > 0 \end{cases} \tag{10}$$

Reference [18] explores alternative formulations of $g(\theta)$ to capture the non-symmetric orientation dependency at shorter separation distances. A summation of higher order terms of the form $\sin(2m\theta)$ is used, which are normalized with respect to the maximum torque angle. It was recently recognized that this function is also polarity dependent, and the coefficients must change with attraction or repulsion much like γ does. Importantly, inclusion of the higher order terms does not affect the sign of $g(\theta)$, which remains positive in the first and third quadrants and negative in the second and fourth quadrants of θ. Using the polarity dependent coefficient γ and function g as described above, we obtain

$$M_C = \begin{cases} \gamma_a f(\phi) g_a(\theta) & \text{for } \phi < 0 \\ \gamma_r f(\phi) g_r(\theta) & \text{for } \phi > 0 \end{cases} \tag{11}$$

where the f function remains $f(\phi) = \phi|\phi|$ and is readily invertible to obtain the required electrostatic potentials for a desired f.

5. ROTATION RATE CONTROL

In this development, the goal is to maintain a constant angular rate of rotation on the cylinder $\dot{\theta}_r$. The error in rotation rate relative to the reference can be defined $\delta\dot{\theta} = \dot{\theta} - \dot{\theta}_r$.

A. CONTROL DEVELOPMENT

For the moment, the disturbance forces are omitted from the system dynamics, which take the form

$$I\ddot{\theta} = \gamma f(\phi) g(\theta) \tag{12}$$

The following energy based positive definite Lyapunov function is chosen:

$$V(\delta\dot{\theta}) = \frac{I}{2}\delta\dot{\theta}^2 \tag{13}$$

The time derivative of this function becomes

$$\dot{V}(\delta\dot{\theta}) = \delta\dot{\theta}(I\ddot{\theta}) \tag{14}$$

$$= \delta\dot{\theta}\left(\gamma f(\phi) g(\theta)\right) \tag{15}$$

where it is assumed $\ddot{\theta}_r = 0$ and the system dynamics from (12) are used. At this point, a control function $f(\phi)$ is chosen, which is implemented via the control voltages $\phi_1 = \phi$ and $\phi_2 = |\phi|$. Similar to the developments in [19], the following control is chosen:

$$f(\phi) = -\frac{f_{\max}}{\pi/2}\text{sign}(g(\theta))\tan^{-1}\left(P\delta\dot{\theta}\right) \tag{16}$$

The arctangent function is used so that the control voltages are smoothly limited at their saturation levels. The sign of $g(\theta)$ is included so that the correct polarity voltage control is utilized in any given quadrant. The resulting Lyapunov rate is

$$\dot{V}(\delta\dot{\theta}) = -\frac{\gamma f_{\max}}{\pi/2}|g(\theta)|\delta\dot{\theta}\tan^{-1}\left(P\delta\dot{\theta}\right) \tag{17}$$

This function is negative semi-definite because $\tan^{-1}(P\delta\dot{\theta})$ has the same sign as $\delta\dot{\theta}$, thus implying global stability to the desired rotation rate. While $g(\theta)$ can be periodically zero, it is not possible for $g(\theta)$ to remain zero unless $\delta\dot{\theta} = 0$ as well. Thus, the largest invariant set where $\dot{V} = 0$ is $\delta\dot{\theta} = 0$, and the system is globally asymptotically stable. Remember that both γ and $g(\theta)$ take different forms depending on whether attractive or repulsive control is used, but their signs are unaffected.

When the experimental testbed disturbance torques are included in the equations of motion, closed-loop rate tracking errors will only be bounded or Lagrange stable. It is not possible to continually compensate for these arresting torques because the control authority via Coulomb charging vanishes at the four equilibrium points ($\theta = n\frac{\pi}{4}$) during every rotation. When the cylinder reaches these orientations, the rotation speed will decrease until control authority is regained, at which point the control law in (16) will raise the rotation rate to match the desired rate. Freeflying spacecraft will not experience significant rotation torques, lending themselves more readily to these control algorithms.

B. EXPERIMENTAL RESULTS

The control algorithm in (16) is implemented on the experimental testbed described above, using the gain $P = 2.0$. As shown in Fig. 7(a), a reference rate $\dot{\theta}_r = 30$ deg/s is prescribed for the first 54 seconds, at which point the reference is changed to $\dot{\theta}_r = -60$ deg/s. The results are compared with a numeric simulation conducted in MATLAB which implements the three sphere MSM, including disturbance torques as described above. There is significantly more error in the rotation rate of the experimental system than in the simulation, which is due to the noise in the magnetic angular encoder and the filtering used to determine the resulting rotation rate. In both the physical system and the simulation, it takes about 8 seconds to attain the 30 deg/s rotation rate, and 18 seconds to reverse the rotation and achieve the 60 deg/s rotation rate in the other direction. Fig. 7(b) shows the Coulomb and disturbance torques (bearing friction and atmospheric drag) as calculated by the simulation. The Coulomb torques are periodic with angular rotation, and sporadic even in the simulation because of the inconsistent control authority as the cylinder rotates through the parallel and perpendicular configurations.

(a) Angular velocity

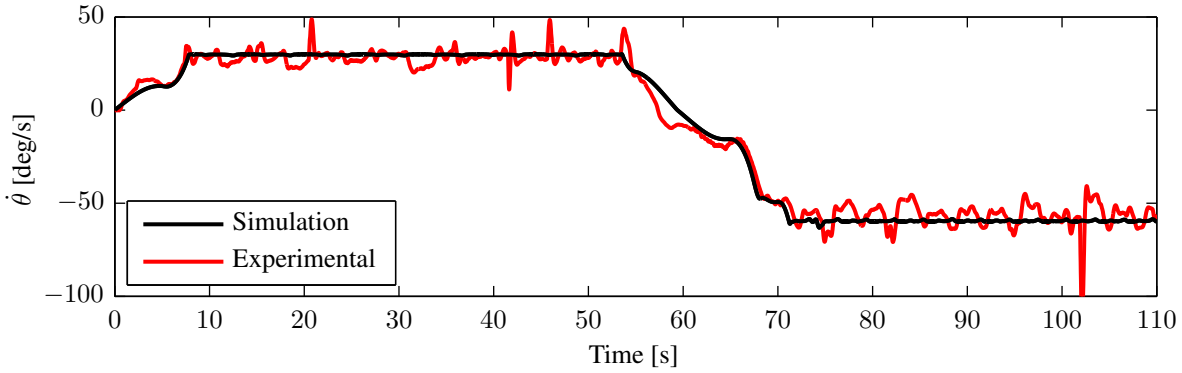

(b) Simulated torques

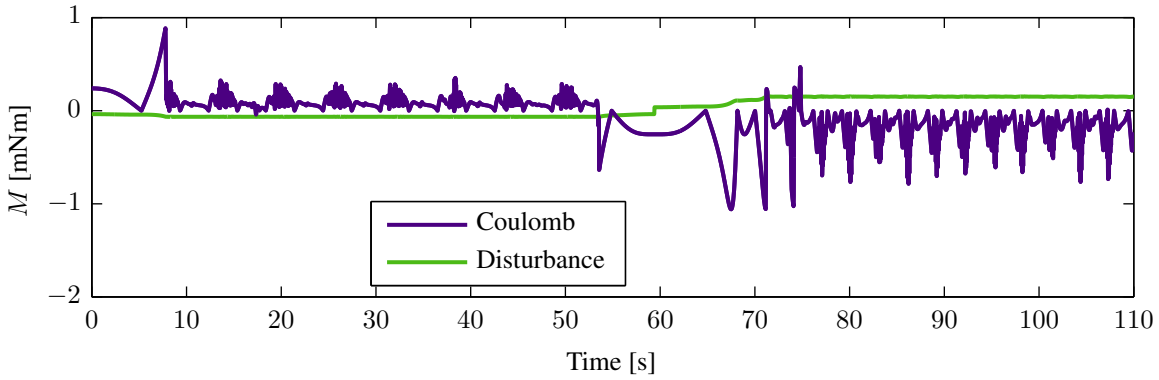

Fig. 7: *Cylinder rotation rate control, experimental and simulation*

6. ATTITUDE CONTROL

Ultimately, the novelty of this testbed is its ability to control the exact attitude of the rotating cylinder. The goal is to track a reference orientation θ_r, or minimize the error in angular position $\delta\theta = \theta - \theta_r$. The reference angle is assumed to be constant, i.e. $\dot{\theta}_r = 0$.

A. CONTROL DEVELOPMENT

The involved nature of the system dynamics that result from the $g(\theta)$ function complicates the stability control arguments. One possible control algorithm has been identified for which local nonlinear stability arguments can be made. The proposed Lyapunov function is:

$$V(\dot{\theta}, \delta\theta) = \frac{1}{2} I\dot{\theta}^2 + \frac{K}{2} g^2(\theta)\delta\theta^2 \tag{18}$$

This function is positive definite only within a given quadrant, as $g^2(\theta)$ vanishes at $\theta = \frac{\pi}{4}$. If the electric potentials are chosen such that

$$f(\phi) = -\frac{1}{\gamma}\left(g(\theta)P\dot{\theta} + g(\theta)K\delta\theta + g'(\theta)\right) \tag{19}$$

where $g'(\theta)$ denotes differentiation with respect to θ, the resulting Lyapunov rate is

$$\dot{V}(\dot{\theta}, \delta\theta) = \dot{\theta}\left(I\ddot{\theta} + Kg(\theta)g'(\theta)\delta\theta^2 + Kg^2(\theta)\delta\theta\right) \tag{20}$$

$$= -g^2(\theta)P\dot{\theta}^2 \tag{21}$$

where several terms cancel when the system dynamics from (12) are included using the control in (19). This Lyapunov rate is negative semi-definite within any quadrant, implying local

stability within that quadrant. The same approach can be taken as in [19] however, where the cylinder is allowed to coast without charge control until it reaches the appropriate quadrant, at which point the attitude control described above is implemented.

The control described above has been shown in simulations to converge to the desired reference attitude, but it is impractical for physical implementation because it requires exact knowledge of the higher order g function as well as its angle derivative. It is preferable to use a control based only on the sign of g, which is readily known for a given quadrant. Moreover, better time performance is provided using a control law of the following form, where K and P are chosen to be positive gains.

$$f(\phi) = -\frac{f_{\max}}{\pi/2}\text{sign}(g(\theta))\tan^{-1}\left[P\delta\dot{\theta} + K\delta\theta\right] \tag{22}$$

The arctangent function is again chosen so that control voltages are smoothly limited to their maximum levels without abrupt saturation. While it is difficult to make Lyapunov stability arguments regarding this nonlinear control, we can analyze the closed loop dynamics, which take the form

$$I\ddot{\theta} = -\frac{\gamma f_{\max}}{\pi/2}|g(\theta)|\tan^{-1}\left[P\delta\dot{\theta} + K\delta\theta\right] \tag{23}$$

If we make the assumption that the reference trajectory is to maintain a constant orientation, i.e. $\dot{\theta}_r = 0$, the closed loop dynamics can be linearized about the reference angle θ_r as follows:

$$\delta\ddot{\theta} + \beta P\delta\dot{\theta} + \beta K\delta\theta = 0 \tag{24}$$

where

$$\beta = \frac{\gamma f_{\max}|g(\theta_r)|}{(\pi/2)I} \tag{25}$$

Note that both γ and $|g(\theta_r)|$ take different forms depending on whether the system is in an electrostatically attractive or repulsive state. Their signs remain unchanged however, and β is always a positive coefficient. Therefore, the roots of this second order differential equation always have negative real components, and the system is assumed to be locally stable in the linearized neighborhood of the reference angle. The natural frequency ω_n and damping coefficient ζ in this vicinity are

$$\omega_n = \sqrt{\beta K} \tag{26}$$

$$\zeta = \frac{P}{2}\sqrt{\frac{\beta}{K}} \tag{27}$$

Because β changes depending on the voltage polarities, the system will have different closed-loop response characteristics (stiffness, damping, etc.) depending on from which direction the cylinder approaches the reference orientation. Linear stability is guaranteed in either case.

B. EXPERIMENTAL RESULTS

The results in Fig. 8 demonstrate the ability to prescribe a specific angular orientation on the rotating cylinder using Coulomb actuation. The cylinder is given an initial rotation rate of 100 deg/s, at which point the charge control algorithm in (22) is implemented via the high voltage power supplies. A reference angle of $\theta_r = 45$ deg is prescribed while the gains are set to $K = 0.08$ and $P = 0.2$. Within 10 seconds the cylinder is brought to rest, and after a slight overshoot, the desired reference angle is achieved to within 1.5 deg. From Fig. 4(a) it can be

seen that it takes 60 seconds for the cylinder to come to rest from this rotation rate by disturbance torques alone. As is evident from Fig. 8(a), the simulation conducted using MATLAB matches the experimental results with formidable accuracy. This simulation implements the full system dynamics using the three sphere MSM, including disturbance torques from bearing and atmospheric drag. Fig. 8(b) depicts the prescribed electric potentials, where blue denotes the sphere voltage ϕ_1 and green denotes the cylinder voltage ϕ_2. Here a slight deviation is evident between the simulation and experiment when the cylinder comes to rest, which is likely the result of sensor noise at low velocities.

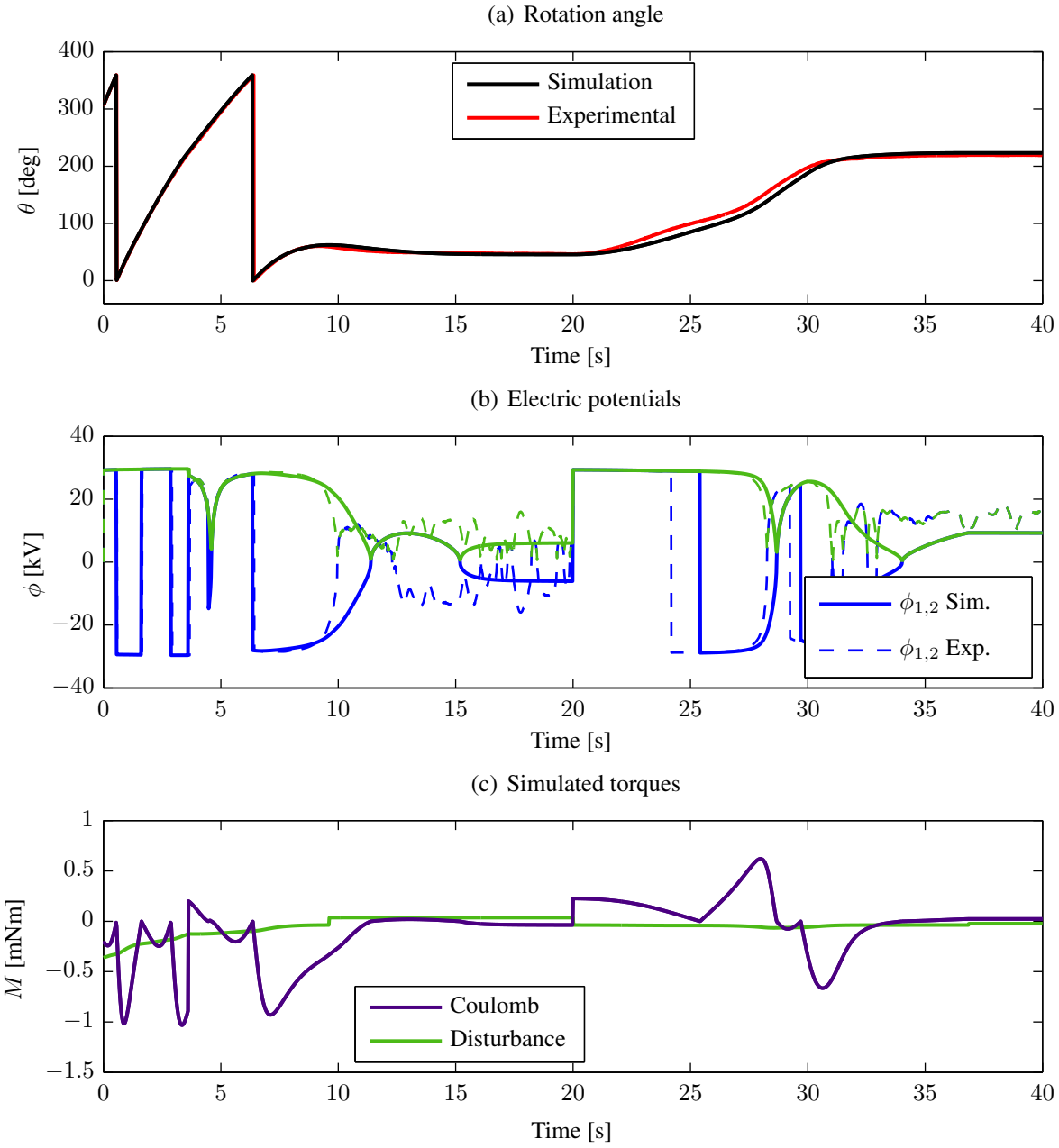

Fig. 8: *Cylinder attitude control: experimental and simulation*

At 20 seconds into the simulation, the reference angle is changed to 225 deg, representing a 180 deg switch in the desired angle. Within 12 seconds the target orientation is achieved, this time with a 5.5 deg attitude error. This is because the reference angle is approached from the direction where repulsive control is required to remove the remaining error, which produces

lower torques than the attractive configuration (as seen in Fig. 6) that are unable to overcome the bearing friction. The simulation demonstrates a lower error of 2 deg, suggesting there is some unmodeled stiction present in the ceramic bearings. Fig. 8(c) displays the friction and Coulomb torques calculated in the simulation, which suggests a maximum Coulomb torque of roughly 1 mNm, which matches well with the results in Fig. 6.

7. CONCLUSION

Improvements have been made on the rotational testbed for verification of remote spacecraft attitude control via Coulomb charging. The new design enables active charging on the rotating object, while the accuracy in the angular position sensing has been improved significantly, and the time delay when switching voltage polarity on the stationary shape has been decreased by an order of magnitude. Moreover, the I/O software is rewritten in NI's Labview, yielding an improved GUI and data acquisition platform. The disturbance torques due to friction in the rotating bearings are characterized along with atmospheric drag and shown to be reduced considerably. While the Multi-Sphere Method remains the best approach for predicting Coulomb torques, a polarity dependent analytic formulation is used to examine the stability of the system. Assuming a frictionless system, as would be the case for free flying spacecraft, globally stable control algorithms are developed for rotation rate control and attitude control. The stability arguments for attitude control are restricted to within a given quadrant of rotation. Physical tracking of rotation rate and exact angular position are demonstrated on the experimental testbed. Besides slight deviations due to angular sensor noise, the experimental results match the numerical simulations extremely well.

ACKNOWLEDGMENTS

This material is based upon work supported by the NASA Science & Technology Research Fellowship (**NASA Grant #NNX11AN47H**).

Thanks to Ian Thom for his assistance in constructing and operating various components of the testbed described herein.

REFERENCES

[1] Cover, J. H., Knauer, W., and Maurer, H. A., "Lightweight Reflecting Structures Utilizing Electrostatic Inflation," US Patent 3,546,706, October 1966.

[2] King, L. B., Parker, G. G., Deshmukh, S., and Chong, J.-H., "Spacecraft Formation-Flying using Inter-Vehicle Coulomb Forces," Tech. rep., NASA/NIAC, January 2002.

[3] Schaub, H., Parker, G. G., and King, L. B., "Challenges and Prospect of Coulomb Formations," *Journal of the Astronautical Sciences*, Vol. 52, No. 1–2, Jan.–June 2004, pp. 169–193.

[4] Stiles, L. A., Seubert, C. R., and Schaub, H., "Effective Coulomb Force Modeling in a Space Environment," *AAS Spaceflight Mechanics Meeting*, Charleston, South Carolina, Jan. 29 – Feb. 2 2012, Paper AAS 12.

[5] Schaub, H. and Sternovský, Z., "Active Space Debris Charging for Contactless Electrostatic Disposal Maneuvers," *6th European Conference on Space Debris*, ESOC, Darmstadt, Germany, April 22–25 2013, Paper No. 6b.O-5.

[6] Hogan, E. and Schaub, H., "Space Weather Influence on Relative Motion Control using the Touchless Electrostatic Tractor," *AAS/AIAA Spaceflight Mechanics Meeting*, Santa Fe, New Mexico, Jan. 26–30 2014, Paper AAS 14-425.

[7] Oltrogge, D. and Finkleman, D., "Consequences of Debris Events in Geosynchronous Orbit," *AIAA/AAS Astrodynamics Specialist Conference*, Honolulu, Hawaii, Aug. 18–21 2008, Paper AIAA 2008–27375.

[8] Anderson, P. V. and Schaub, H., "Local Debris Congestion in the Geosynchronous Environment With Population Augmentation," *6th European Conference on Space Debris*, ESOC, Darmstadt, Germany, April 22–25 2013, Paper No. 3a.P-3.

[9] Hoots, F. and Hansen, B., "COBRA: A Covariance-Based Debris Risk Assessment Model," *AAS/AIAA Astrodynamics Specialists Conference*, Hilton Head, SC, Aug. 11–15 2013, Paper No. AAS 13-843.

[10] Hansen, B., "Summarizing the General Effects of Breakup Debris in GEO," *AAS/AIAA Astrodynamics Specialists Conference*, Hilton Head, SC, Aug. 11–15 2013, Paper No. AAS 13-844.

[11] Schaub, H. and Moorer, D. F., "Geosynchronous Large Debris Reorbiter: Challenges and Prospects," *The Journal of the Astronautical Sciences*, Vol. 59, No. 1–2, 2014, pp. 161–176.

[12] Hogan, E. and Schaub, H., "Relative Motion Control for Two-Spacecraft Electrostatic Orbit Corrections," *AIAA Journal of Guidance, Control, and Dynamics*, Vol. 36, No. 1, Jan. – Feb. 2013, pp. 240–249.

[13] Papushev, P., Karavaev, Y., and Mishina, M., "Investigations of the evolution of optical char- acteristics and dynamics of proper rotation of uncontrolled geostationary artificial satellites," *Advances in Space Research*, Vol. 43, 2009.

[14] Rembala, R., Teti, F., and Couzin, P., "Operations Concept for the Robotic Capture of Large Orbital Debris," *35th Annual AAS Guidance & Control Conference*, AAS, Breckenridge, Colorado, February 3–8 2012, Paper No. AAS 12-018.

[15] Couzin, P., Teti, F., and Rembala, R., "Active Removal of Large Debris : Rendez-vous and Robotic Capture Issues," *2nd European Workshop on Active Debris Removal*, Paris, France, 2012, Paper #7.5.

[16] Jasper, L. E. Z. and Schaub, H., "Effective Sphere Modeling for Electrostatic Forces on a Three-Dimensional Spacecraft Shape," *AAS/AIAA Spaceflight Mechanics Meeting*, Girdwood, Alaska, July 31 – August 4 2011, Paper AAS 11–465.

[17] Hogan, E. A. and Schaub, H., "Impacts of Tug and Debris Sizes on Electrostatic Tractor Charging Performance," *International High Power Laser Ablation and Beamed Energy Propulsion*, Santa Fe, New Mexico, April 21–25 2014.

[18] Bennett, T. and Schaub, H., "Touchless Electrostatic Three-Dimensional Detumbling of Large GEO Debris," *AAS/AIAA Spaceflight Mechanics Meeting*, Santa Fe, New Mexico, Jan. 26–30 2014, Paper AAS 14-378.

[19] Schaub, H. and Stevenson, D., "Prospects Of Relative Attitude Control Using Coulomb Actuation," *Jer-Nan Juang Astrodynamics Symposium*, College Station, TX, June 25–26 2012, Paper AAS 12–607.

[20] Stevenson, D. and Schaub, H., "Terrestrial Testbed for Remote Coulomb Spacecraft Rotation Control," *International Journal of Space Science and Engineering*, Vol. 2, No. 1, 2014, pp. 96–112.

[21] Wang, S., "Shape control of charged spacecraft cluster with two or three nodes," 2010.

[22] Seubert, C. R. and Schaub, H., "Electrostatic Force Model for Terrestrial Experiments on the Coulomb Testbed," *61st International Astronautical Congress*, International Astronautical Federation, Prague, CZ, Sept. 2010, Paper IAC-10.C1.1.9.

[23] Stevenson, D. and Schaub, H., "Multi-Sphere Method for Modeling Spacecraft Electrostatic Forces and Torques," *Advances in Space Research*, 2012.

[24] Stevenson, D. and Schaub, H., "Optimization of Sphere Population for Electrostatic Multi Sphere Model," *IEEE Transactions on Plasma Science*, Vol. 41, No. 12, Dec. 213, pp. 3526–3535.

[25] Smythe, W. R., *Static and Dynamic Electricity*, McGraw–Hill, 3rd ed., 1968.

[26] Sliško, J. and Brito-Orta, R. A., "On approximate formulas for the electrostatic force between two conducting spheres," *American Journal of Physics*, Vol. 66, No. 4, 1998, pp. 352–355.